Supplementary Information

Rational integration of fluorine and hydroxyl functionalities in UiO-66 metal–organic framework for enhanced propylene/propane separation

Yao-Ting Wang,[ab] Yu-Tung Chou,[ab] Po-Chuan Chao,[ab] Anton S. Pozdeev,[c] Alexander S. Ivanov,[d] Yu-Chun Chuang,[e] Chung-Kai Chang,[e] Ilja Popovs,[d] Watchareeya Kaveevivitchai*[abf] and Teng-Hao Chen*[g]

[a] Department of Chemical Engineering, National Cheng Kung University, Tainan City 70101, Taiwan

[b] Center for Resilience and Intelligence on Sustainable Energy Research (RiSER), National Cheng Kung University, Tainan City 70101, Taiwan

[c] Department of Chemical & Biomolecular Engineering, Vanderbilt University, Nashville, TN 37235, USA

[d] Department of Nuclear Engineering, University of Tennessee, TN 37996, USA

[e] National Synchrotron Radiation Research Center, Hsinchu City 300092, Taiwan

[f] Academy of Innovative Semiconductor and Sustainable Manufacturing, National Cheng Kung University, Tainan City 70101, Taiwan

[g] School of Pharmacy, National Cheng Kung University, Tainan City 70101, Taiwan

*To whom correspondence should be addressed. E-mail: wkaveechai@mail.ncku.edu.tw, thchen@gs.ncku.edu.tw

General Methods and Materials

All starting materials and solvents were obtained from commercial suppliers (Sigma-Aldrich and TCI) and used without further purification. Powder X-ray diffraction (PXRD) patterns were collected on a Bruker D8 Advance diffractometer using Cu Kα radiation (λ = 1.5406 Å). Ultrahigh purity gases N_2 (99.9995%), C_3H_6 (99.9%), C_3H_8 (99.9%), and He (99.9995%) were purchased from Yun Shan, Ltd. (Taiwan). Thermogravimetric analysis (TGA) was performed on a Mettler Toledo TGA 2 Star System under N_2 flow, typically from 50 to 800 °C at a heating rate of 10 °C min^{-1}. Supercritical CO_2 activation was conducted using a Tousimis SAMDRI-PVT-3D critical-point dryer with liquid CO_2 at 40 °C and 1200 psi. Fourier-transform infrared (FT-IR) spectra were collected on a Bruker Alpha II spectrometer in the 400–4000 cm^{-1} range. *In situ* synchrotron PXRD experiments were conducted at the TPS-19A beamline of the National Synchrotron Radiation Research Center (NSRRC) in Hsinchu, Taiwan, to monitor structural changes under varying gas atmospheres. Scanning electron microscopy (SEM) images were obtained using a Hitachi SU8000 field-emission scanning electron microscope (FE-SEM).

Synthesis of UiO-66-F_4[1]

UiO-66-F_4 was synthesized following a published method. The zirconyl nitrate hydrate ($ZrO(NO_3)2{\cdot}xH_2O$, 45 mg, 0.19 mmol) was mixed in 2 mL of DI water and 500 µL of AcOH via sonication for 15 min. Separately, the 2,3,5,6-tetrafluorobenzene-1,4-dicarboxylic acid (F_4-BDC) (30 mg, 0.12 mmol) was mixed in 1 mL of DI water via sonication for 15 min. The two solutions were mixed and stirred at room temperature for 40 h. The powders were collected by centrifugation (6,000 rpm for 10 min). The powders were washed with 3 × 10 mL of DI water and then subsequently washed with 2 × 10 mL of EtOH. The powder was dried in a vacuum oven at 60 °C overnight, and the yield was 80% based on Zr. The activation method involved soaking the as-synthesized sample in DI water for 1 d, with the water being refreshed every 3 h. The sample was subjected to liquid nitrogen for one min, then placed in a freeze dryer at −85 °C for 24 h.

Synthesis of UiO-66-$(OH)_2$[2]

2,5-Dihydroxybenzene-1,4-dicarboxylic acid ($(OH)_2$-BDC) (30 mg, 0.15 mmol), and $ZrCl_4$ (45 mg, 0.19 mmol) were mixed in 6 mL of DI water and 4 mL of AcOH in a 20 mL glass vial. The mixture was sonicated for 15 min and then placed in an oven at 100 °C for 20 h. The powders were collected by centrifugation (6,000 rpm for 10 min). The powders were washed with 3 × 10 mL of DI water and then subsequently washed with 3 × 10 mL of EtOH. The powder was dried in a vacuum oven at 60 °C overnight, and the yield was 66% based on Zr. The sample was immersed in ethanol for 1 d, with the solvent being changed every 3 h, followed by soaking in acetone for 1 d, with the solvent being changed every 3 h. Then, the sample was dried in a vacuum oven at 120 °C overnight.

Synthesis of UiO-66-$F_2(OH)_2$

The $ZrO(NO_3)_2 \cdot xH_2O$ (45 mg, 0.19 mmol) was dissolved in a mixture of 1 mL of DI water and 500 µL of AcOH via sonication for 15 min. The mixture was placed in a 60 °C oven for 12 h to obtain a zirconium cluster solution. Separately, 3,6-difluoro-2,5-dihydroxybenzene-1,4-dicarboxylic acid ($F_2(OH)_2$-BDC)[3] (30 mg, 0.14 mmol) was dissolved in 1 mL of DI water via sonication for 15 min. The two solutions were mixed and stirred at room temperature for 48 h. The powders were collected by centrifugation (6,000 rpm for 10 min). The powders were washed with 3 × 10 mL of DI water and then subsequently washed with 2 × 10 mL of EtOH. The powder was dried in a vacuum oven at 60 °C overnight, and the yield was 66% based on Zr. The activation method involved soaking the as-synthesized sample in DI water for 1 d, with the water being refreshed every 3 h. The sample was subjected to liquid nitrogen for one min, then placed in a freeze dryer at −85 °C for 24 h.

Supercritical CO_2 ($ScCO_2$) Drying

$ScCO_2$ drying was conducted using the Tousimis Samdri PVT-3D critical point dryer. The samples were soaked in absolute ethanol (EtOH) for 1 d, with the EtOH solution being replaced every 3 h. After removing the excess EtOH, the samples were transferred to the supercritical CO_2 dryer. The chamber was filled with liquid CO_2 and maintained at 0 °C for 1 h. The samples underwent a venting and bleeding process, which was repeated three times, with each cycle lasting 15 min. Once all the valves were closed, the temperature was raised to approximately 40 °C. After bleeding off CO_2 for 12 h, the samples were transferred to a vial filled with N_2.

Gas Adsorption Measurements

Gas adsorption isotherms were measured using a Micromeritics 3Flex high-performance gas adsorption analyzer. Approximately 100 mg of the activated sample was degassed under vacuum at 393 K for 12 h before measurement. Each sample tube was capped, evacuated to 1×10^{-5} Torr, and heated to 393 K for 4 h. Isotherms were collected at 298 K over a pressure range of 0 to 760 mmHg. Ultra-high-purity gases, including N_2 (99.9995%), C_3H_6 (99.9%), C_3H_8 (99.9%), and He (99.9995%), were used for free-space corrections and adsorption experiments.

Isosteric Heat of Adsorption (Q_{st})

The isosteric heat of adsorption (Q_{st}) was calculated from adsorption isotherms collected at 283, 298, and 308 K using the Clausius–Clapeyron relation, as commonly applied in physisorption systems:[4]

$$Q_{st} = RT^2 \left(\frac{\partial \ln(P)}{\partial T} \right)_q$$

where R is the universal gas constant (8.314 J mol^{-1} K^{-1}), ln (P) is the natural logarithm of pressure (mmHg), and T is the temperature (K).

IAST Selectivity Calculations

Ideal adsorbed solution theory (IAST) selectivities for equimolar C_3H_6/C_3H_8 mixtures were calculated using pure-component isotherms fitted by the dual-site Langmuir-Freundlich (DSLF) model.

The selectivity (S) is defined as:[5]

$$S = \frac{(x_1/y_1)}{(x_2/y_2)}$$

Where x_i and y_i are the mole fractions of component i in the adsorbed and gas phases, respectively, under equilibrium conditions.

Breakthrough Experiments

Dynamic gas separation measurements were carried out using a PSA-300LC system (L&C Science and Technology, Hialeah, FL, USA). Approximately 1.2 g of UiO-66-$F_2(OH)_2$ was packed into a stainless-steel column (4 mm × 150 mm). Before each run, the column was activated at 393 K under vacuum for 8 h and then purged with He (10 mL min^{-1}) at 298 K for 5 min. Binary gas mixtures (C_3H_6/C_3H_8, 50/50 v/v) were introduced at a flow rate of 3 mL min^{-1} and a pressure of 1 bar, and evaluated through five consecutive dynamic breakthrough experiments. The effluent composition was analyzed continuously using a mass spectrometer (Extorr XT-100).

Computational Details

Periodic density functional theory (DFT) calculations were performed using the Vienna *Ab initio* Simulation Package (VASP).[6] The exchange–correlation energy was calculated using the generalized gradient approximation (GGA) of Perdew–Burke–Ernzerhof (PBE) functional.[7] Long-range dispersion interactions were included using Grimme's D3 correction with Becke–Johnson damping (D3(BJ)),[8] which is essential for accurately describing hydrocarbon adsorption in porous materials.

Structural optimizations were performed using the conjugate gradient algorithm (IBRION = 2), allowing full relaxation of atomic positions and lattice parameters (ISIF = 3). The plane-wave kinetic energy cutoff was set to 600 eV with precision set to Accurate. Electronic self-consistency was achieved with an energy convergence criterion of 1×10^{-7} eV. Geometry optimization was considered converged when the residual forces on all atoms were below 0.02 eV $Å^{-1}$. Given the relatively large size of the UiO-66-$F_2(OH)_2$ unit cell, the Brillouin zone was sampled using a Γ-centered (1 × 1 × 1) k-point mesh.

The experimentally determined structure of UiO-66-$F_2(OH)_2$ was used as the starting model (see Table S1 for the full comparison of the DFT-optimized lattice parameters and experimental data). A single guest molecule (C_3H_6 or C_3H_8) was introduced into the pore of the primitive cell. For each adsorbate, we performed geometry optimization for six independent initial configurations with randomized positions and orientations to identify the most energetically stable adsorption geometry.

The adsorption interaction energy for the most energetically stable structures was calculated as:

$$\Delta E = E_{\mathrm{MOF+guest}} - E_{\mathrm{MOF}} - E_{\mathrm{guest}}$$

where $E_{\mathrm{MOF+guest}}$ is the total energy of the optimized adsorption complex, E_{MOF} is the energy of the relaxed empty framework, and E_{guest} is the energy of the isolated gas molecule.

Table S1. Lattice parameters of the UiO-66-$F_2(OH)_2$ crystal structure obtained by X-ray diffraction and DFT calculations.

	a(Å)	b(Å)	c(Å)	α(°) = β(°) = γ(°)
X-ray crystallography	20.81	20.81	20.81	90.0
DFT/PBE-D3(BJ)	21.19	21.19	21.19	90.0

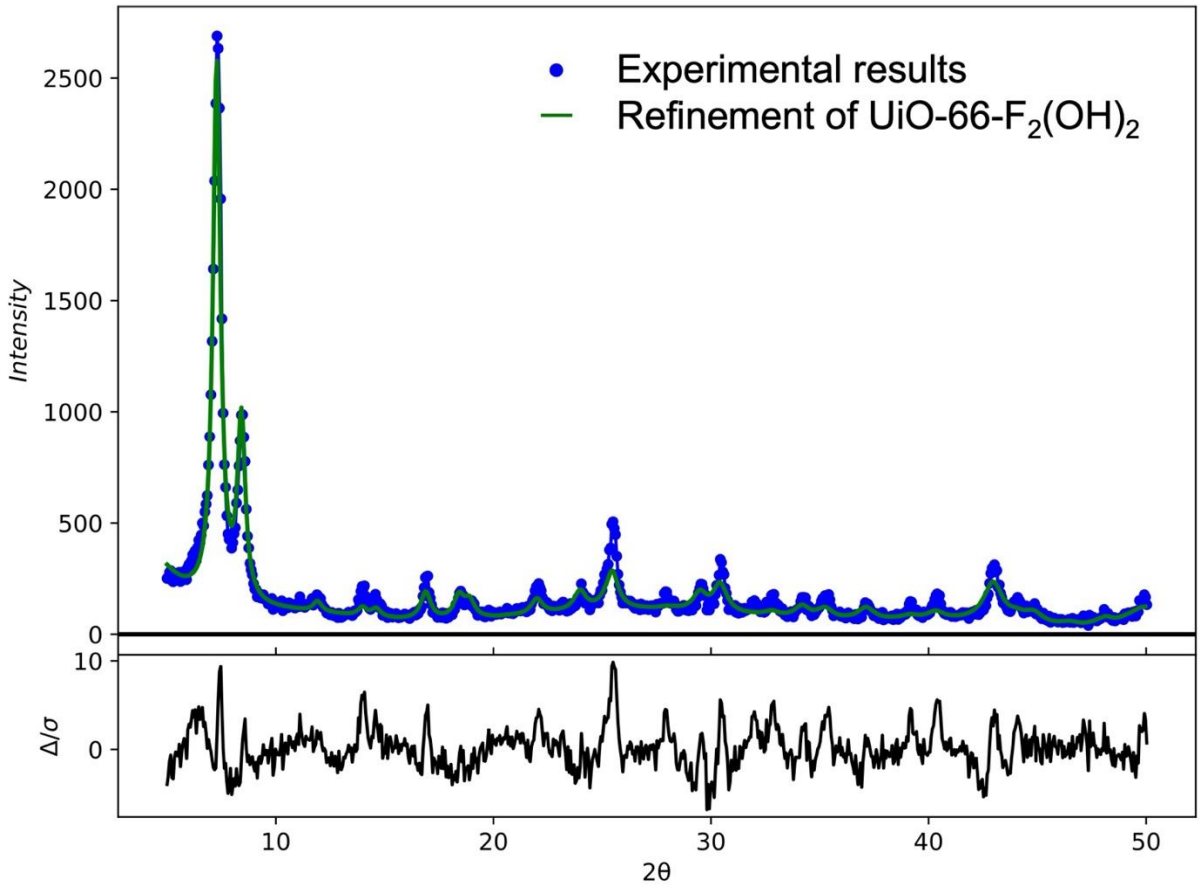

wR:13.811	R_f:8.892	GOF: 1.82
Unit cell:		
a: 20.87	b: 20.87	c: 20.87

Fig. S1 Rietveld refinement of the PXRD pattern for UiO-66-$F_2(OH)_2$. The experimental data (blue circles), calculated profile (green line), and difference curve (black line) are shown.

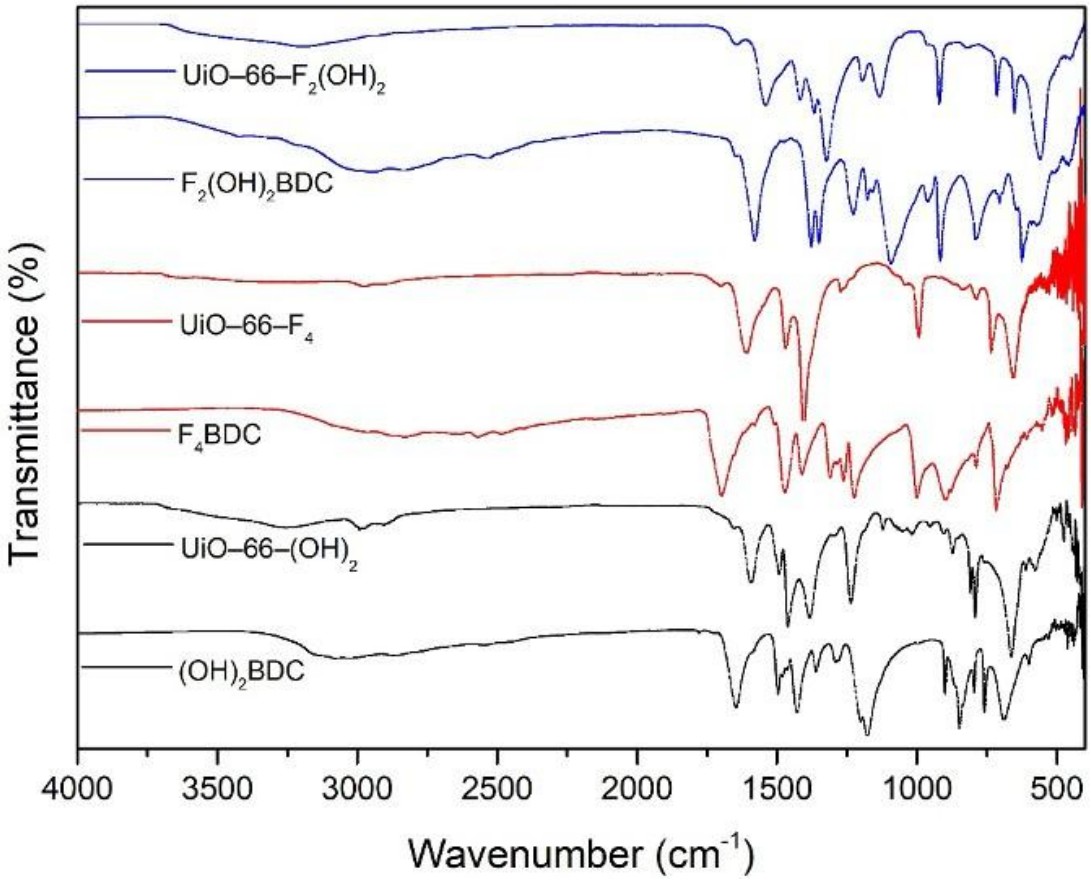

Fig. S2 FT-IR spectra of UiO-66-F_4, -$(OH)_2$, -$F_2(OH)_2$, and their organic ligands.

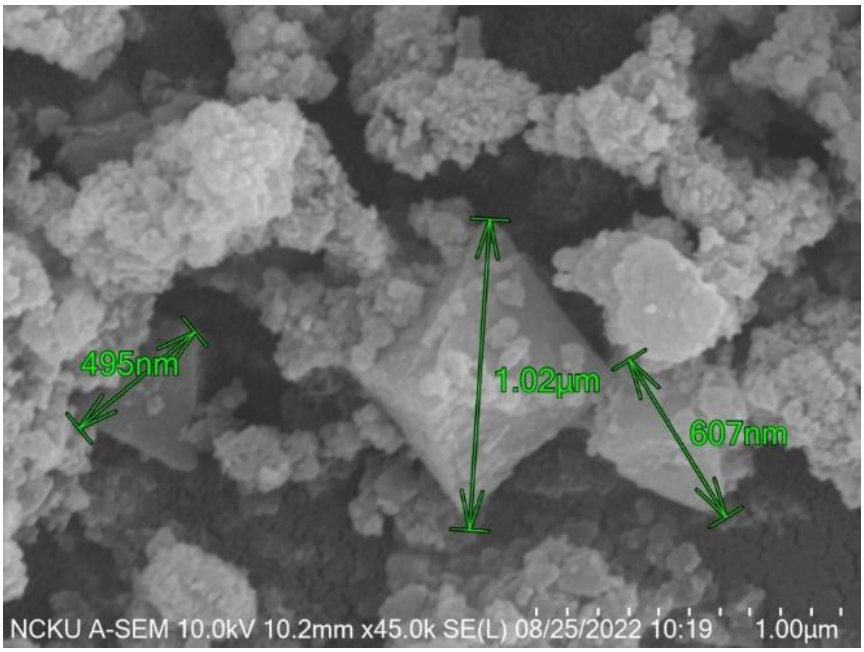

Fig. S3 SEM image of UiO-66-$F_2(OH)_2$.

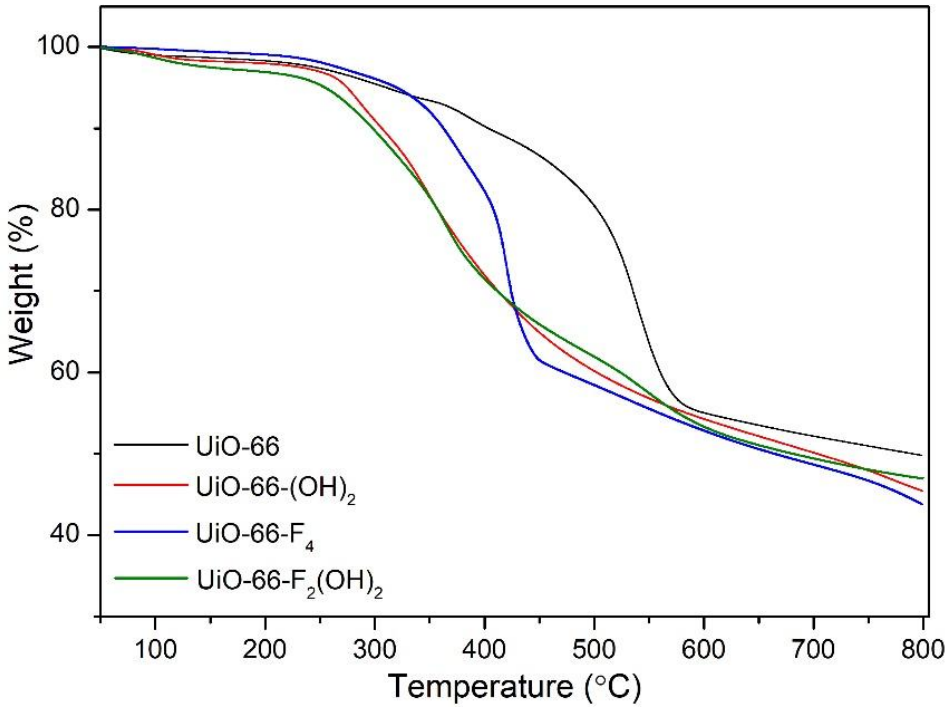

Fig. S4 TGA curves of UiO-66 derivatives.

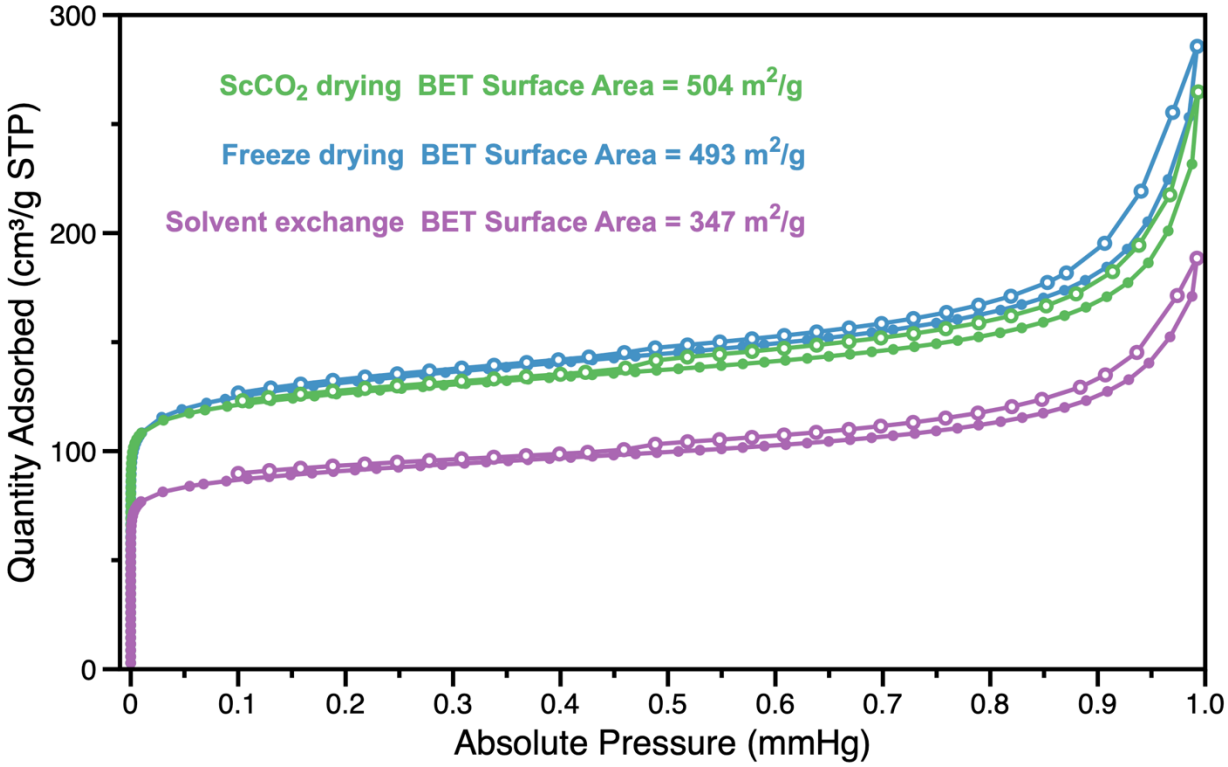

Fig. S5 77 K N_2 adsorption (filled) and desorption (empty) isotherms of UiO-66-$F_2(OH)_2$ obtained through different activation methods.

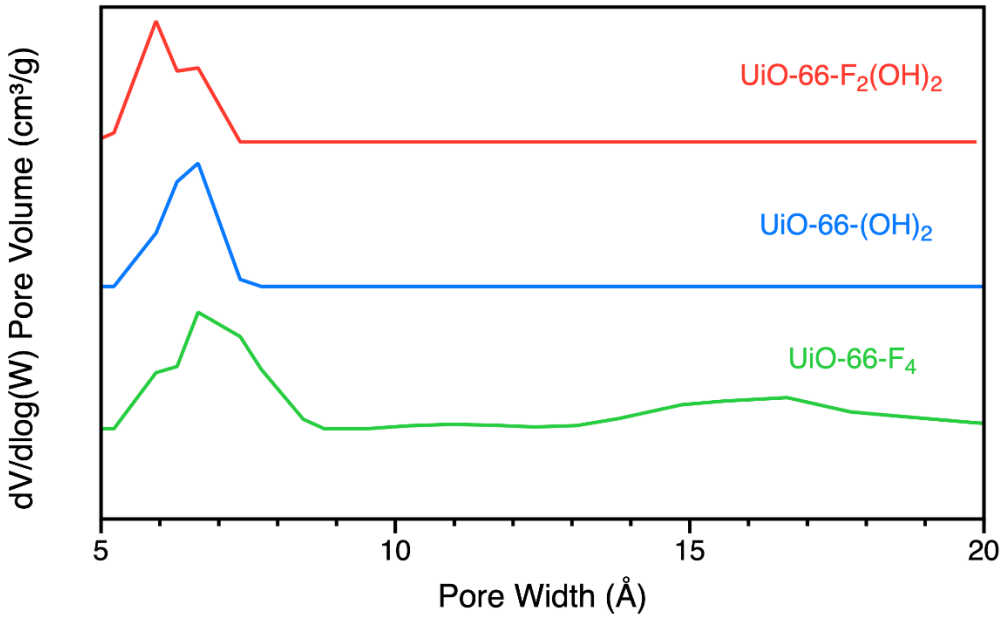

Fig. S6 Pore size distributions of UiO-66 derivatives.

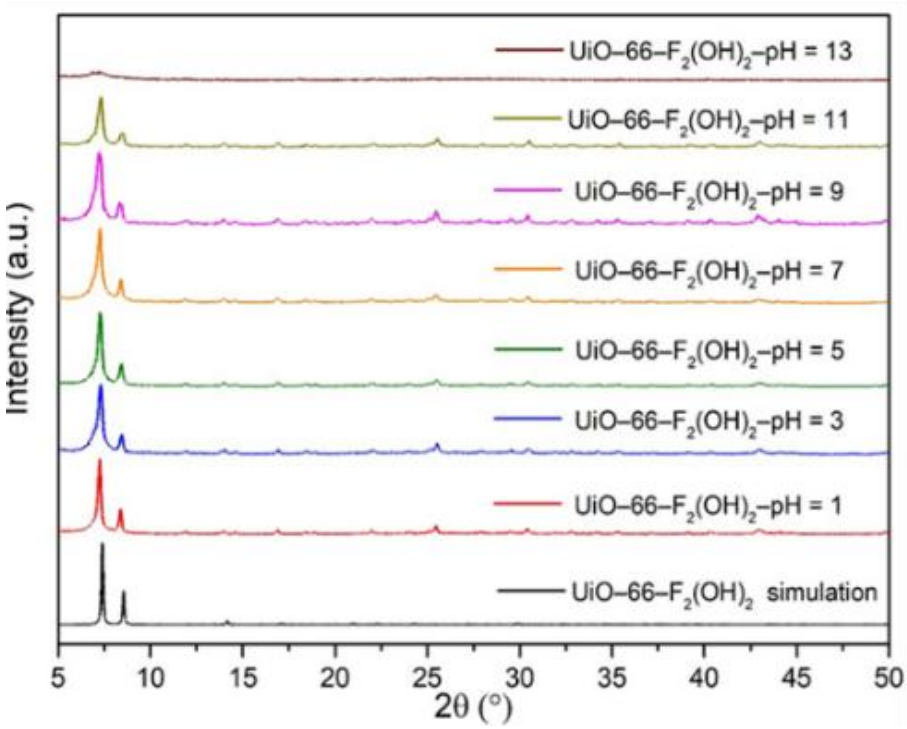

Fig. S7 PXRD patterns of UiO-66-$F_2(OH)_2$ in aqueous solutions at various pH values for 7 d.

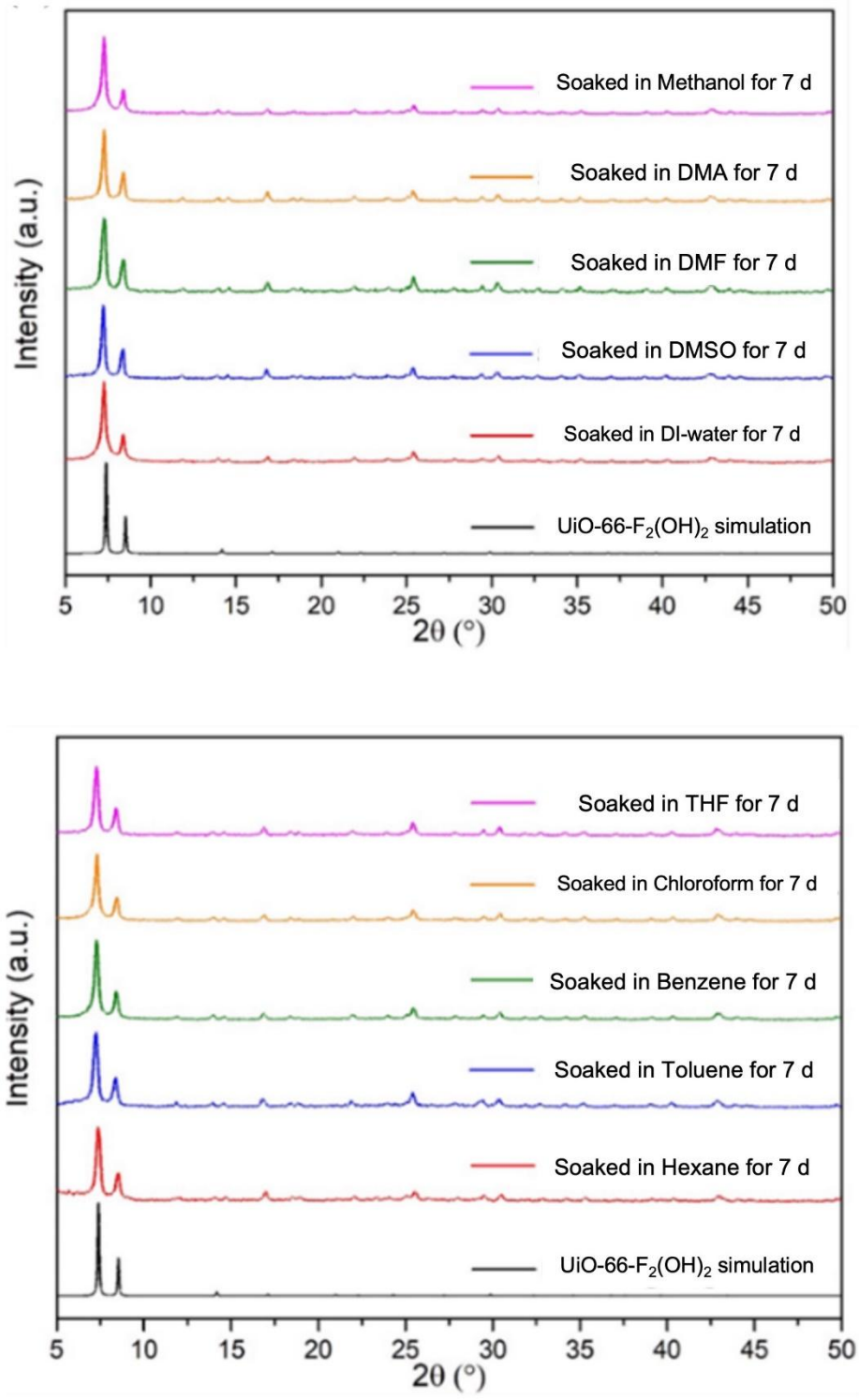

Fig. S8 PXRD patterns of UiO-66-$F_2(OH)_2$ after soaking in various solvents for 7 d.

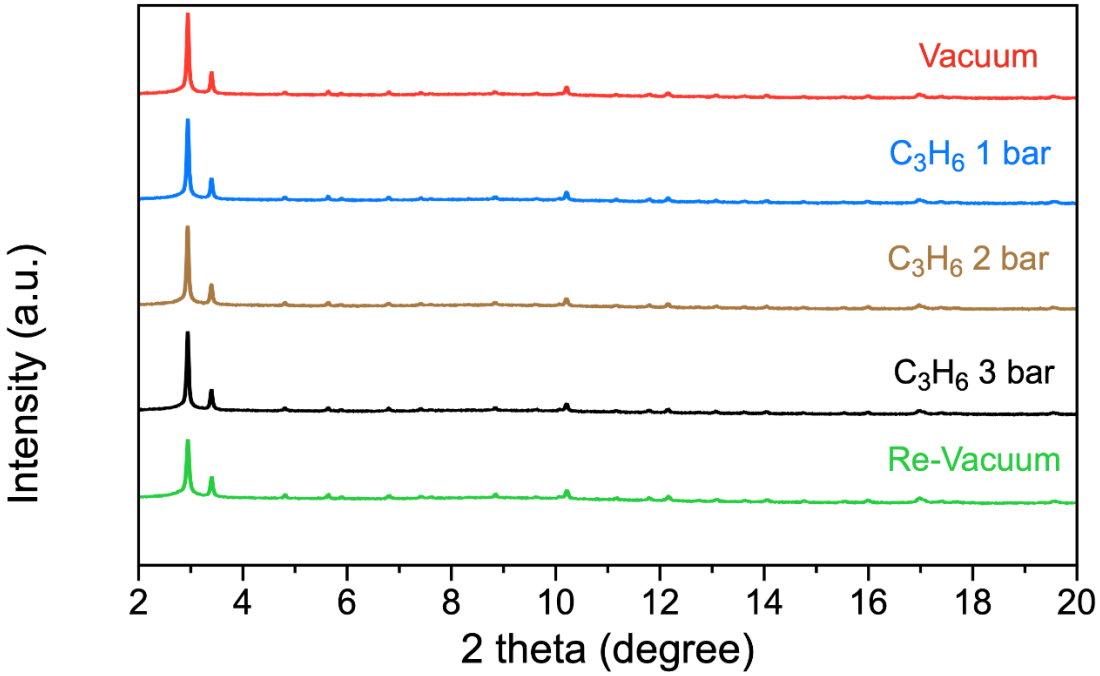

Fig. S9 *In situ* synchrotron PXRD patterns of UiO-66-$F_2(OH)_2$ upon C_3H_6 uptake at different pressures.

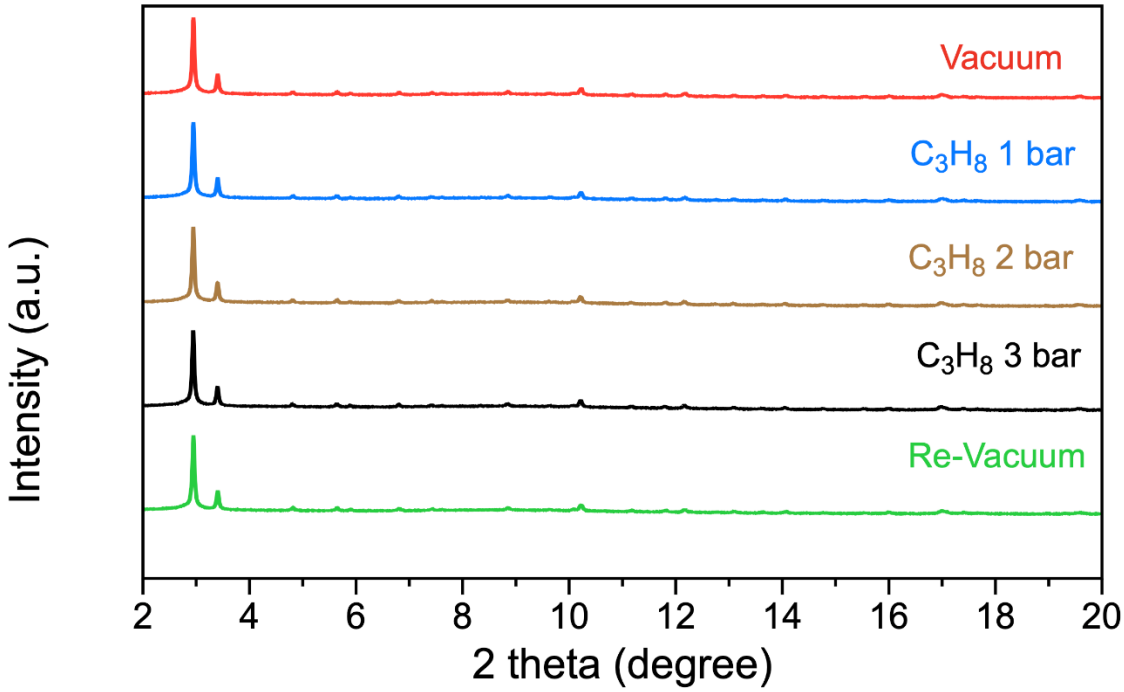

Fig. S10 *In situ* synchrotron PXRD patterns of UiO-66-$F_2(OH)_2$ upon C_3H_8 uptake at different pressures.

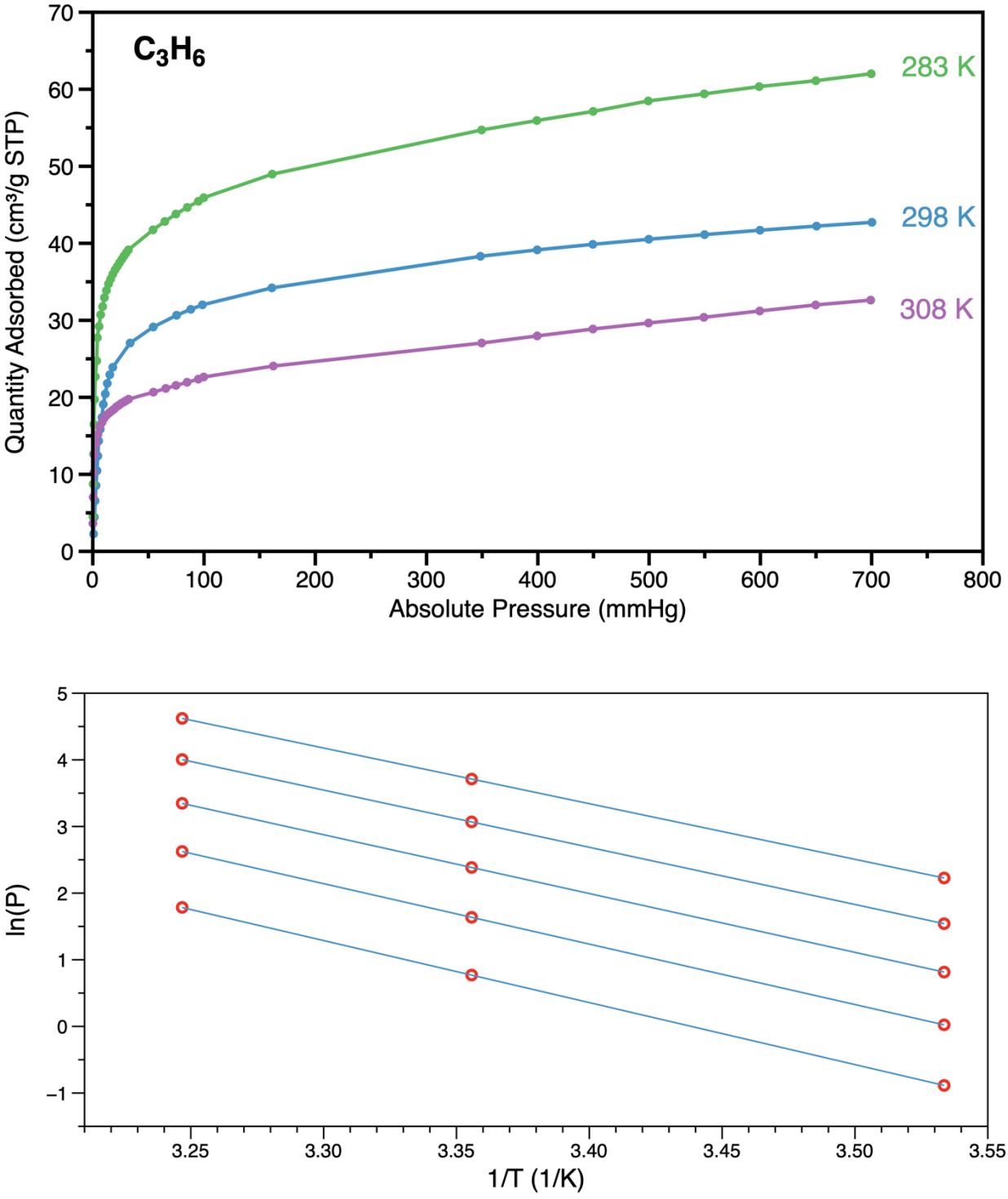

Fig. S11 C_3H_6 sorption isotherms (top) and isostere plot (ln(*P*) against 1/*T*) (bottom) of UiO-66-$F_2(OH)_2$ at 283, 298, and 308 K for the calculation of Q_{st}.

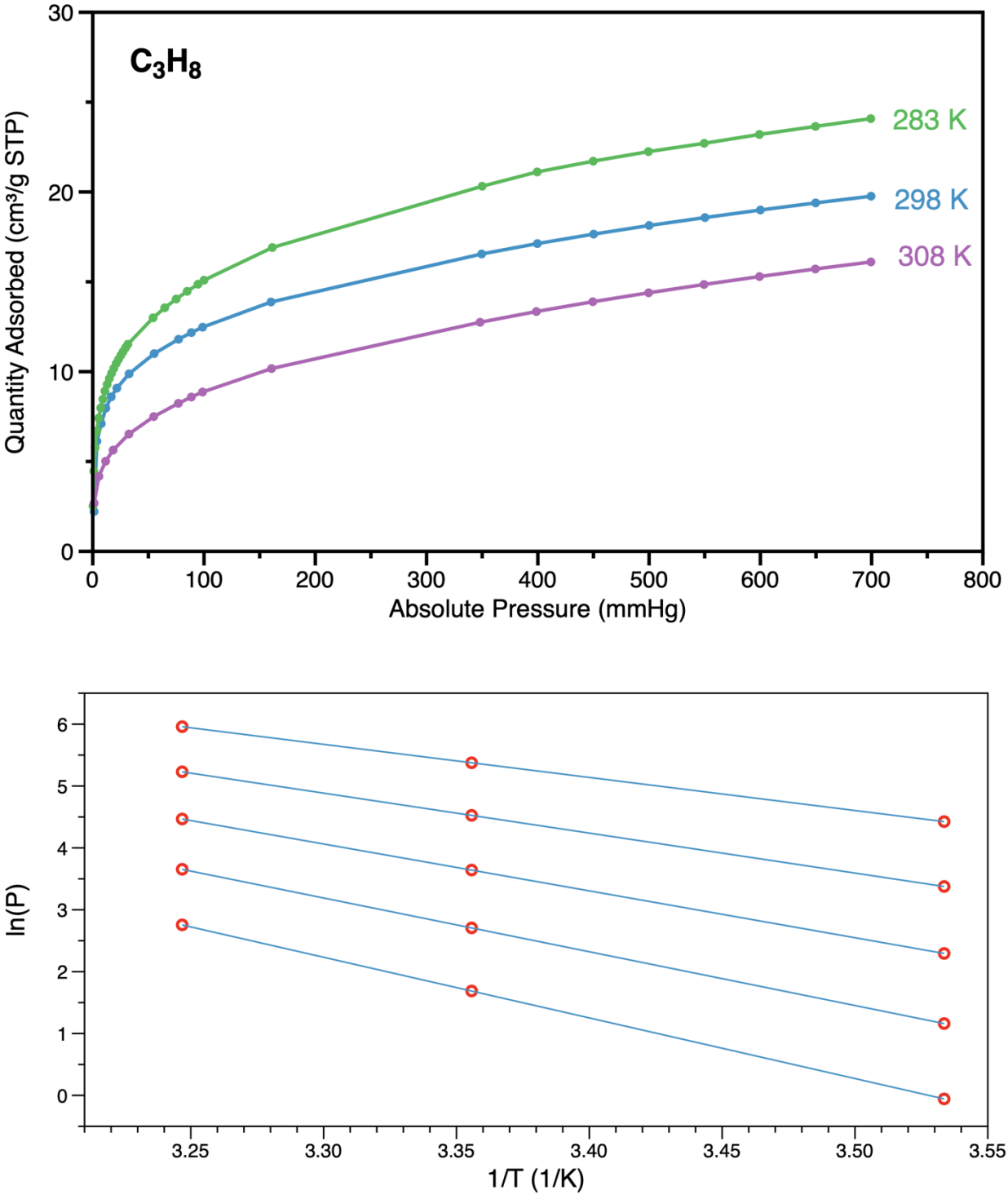

Fig. S12 C_3H_8 sorption isotherms (top) and isostere plot (ln(*P*) against 1/*T*) (bottom) of UiO-66-$F_2(OH)_2$ at 283, 298, and 308 K for the calculation of Q_{st}.

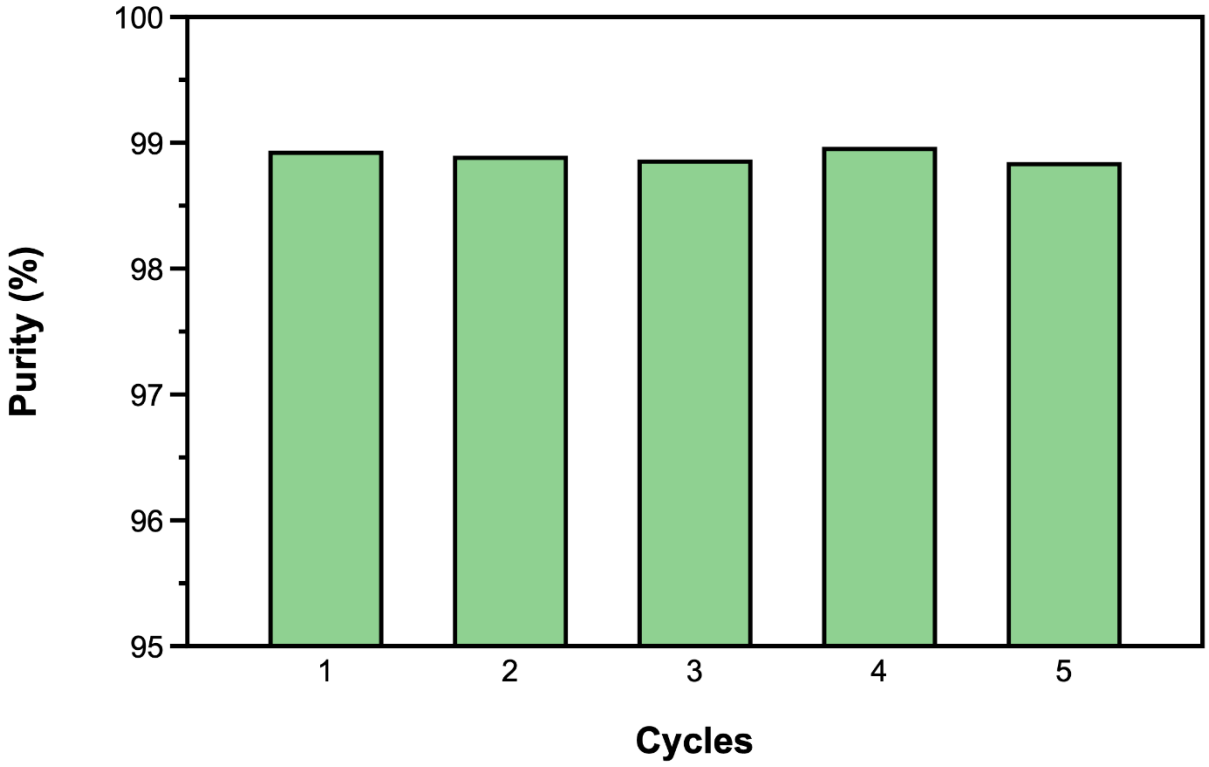

Fig. S13 The purity of eluted C_3H_8 from breakthrough experiments.

Reference:

1. Z. Chen, X. Wang, H. Noh, G. Ayoub, G. W. Peterson, C. T. Buru, T. Islamoglu and O. K. Farha, *CrystEngComm*, 2019, **21**, 2409–2415.
2. Z. H. Rada, H. R. Abid, J. Shang, H. Sun, Y. He, P. Webley, S. Liu and S. Wang, *Ind. Eng. Chem. Res.*, 2016, **55**, 7924–7932.
3. R. Anbazhagan, T.-S. Wang, H.-P. Kuan, I. Popovs, H.-K. Liu, T.-L. Hung, W. Kaveevivitchai and T.-H. Chen, *Chem. Asian J.*, 2025, **20**, e202401329.
4. B. Xu, H. Duan, M. Chu, G. Cao and Y. Yang, *J. Mater. Chem. A.*, 2013, **1**, 4565–4570.
5. K. S. Walton and D. S. Sholl, *AlChE J.*, 2015, **61**, 2757–2762.
6. G. Kresse and J. Hafner, *Phys. Rev. B*, 1993, **47**, 558–561.
7. J. P. Perdew, K. Burke and M. Ernzerhof, *Phys. Rev. Lett.*, 1996, **77**, 3865–3868.
8. S. Grimme, J. Antony, S. Ehrlich and H. Krieg, *J. Chem. Phys.*, 2010, **132**, 154104.